6 mm, and length of 70 cm, allowing the working gas to flow through. The copper tape electrode that encircled the outer part of the tube was connected to the ground. We introduced helium (purity, 99.999%) working gas into the annular space. By supplying the power, a nonequilibrium APP stream was stably confined in the annular space, with a flow rate of 400 standard cubic centimeters per minute (sccm) moving through the 70-cm long capillary. The helium carrier gas passed through the precursor recipient that contained TEOS, bubbled, and was introduced into the plasma plume. We varied the position of the precursor inlet either before the discharge zone (Fig. 1[a]) or at 10 cm before the outlet nozzle (Fig. 1[b]).

A. Attenuated Total-Reflection–FTIR Spectroscopy

The chemical composition of the films was characterized using a Bruker VERTEX-70 (Bruker Optik GmbH, Ettlingen, Germany) FTIR spectrophotometer equipped with a single-reflection attenuated total-reflection (ATR) accessory that used a germanium crystal as an internal reflection element. IF absorbance spectra were recorded in the 400−4000 cm^{-1} range, with a resolution of 4 cm^{-1}. Before each sample scan, the signal of the bare substrate was taken as reference. We performed baseline correction using Bruker's OPUS 6.5 software after 200 scans of each sample.

B. Field-Emission Scanning Electron Microscopy

We studied the morphology of SiO_x films using field-emission scanning electron microscopy (FE-SEM). FE-SEM images were taken using a Zeiss Ultra 55 FE-SEM with a Gemini column on carbon-coated surfaces by sputter coating (108 Auto Cressington sputter coater; Redding, CA).

C. Culture and Preparation of CT-26 Cells

We performed cellular adhesion tests using CT-26 (colon cancer) cells. Cells were cultured in Dulbecco's Modified Eagle's Medium (DMEM), which we supplemented with 1% volume/volume antibiotics (10,000 U/mL penicillin G sodium and 10 mg/mL streptomycin), 2 mM L-glutamine (Fisher Scientific; Illkirch-Graffenstaden, France), and 10% fetal bovine serum (FBS; Sigma-Aldrich, Lyon, France). Cells were expanded by routine cell-culture techniques in 25-cm^2 cell-culture flasks, containing 5 mL 10% serum supplemented medium. We incubated the cells in a humidified atmosphere of 95% air and 5% CO_2 for 24 h at 37°C.

When seeded out for experiments, the cells were detached by trypsinization, pelleted (1 mL for 3 min with a table centrifuge; Beckman Coulter; Fullerton, CA), and resuspended in complete growth medium. We counted the number of cells in the suspension using a C chip (DHC-F01; Biochrom, Berlin, Germany). We then seeded 5 mL of CT-26 cell suspension with a density of 105/tube into the noncoated and coated tubes

that were incubated at physiological conditions for 48 h. After 48 h, the cells were detached by trypsinization and counted with the C chip.

III. RESULTS AND DISCUSSION

A. Influence of Process Parameters on SiO_x Film Deposited on Samples Placed outside of the Tube

We prepared the SiO_x thin films on the Si (100) substrates that we placed outside of the jet by PECVD, using TEOS as the precursor at atmospheric pressure. The experimental apparatus that was used in this step is schematically shown in Fig. 1(a). As the carrier gas, we used helium with a flow rate of 400 sccm. TEOS flow was 0.2 sccm. Substrate distance from the nozzle outlet varied from 5 to 20 mm. The Si (100) samples were ultrasonically cleaned in an acetone bath for 30 min and soaked in ethanol for 30 min. After these steps, samples were rinsed in deionized water. The cleaned Si wafers were air dried and then used for measurements.

The coated films were analyzed for film thickness, morphology, and composition, and we used FE-SEM to examine film-surface morphology. hemical compositions of the thin films were determined using FTIR spectroscopy. Figure 2(a) shows the FTIR spectrometric analysis of the atmospheric plasma jet–deposited SiO_x films for the setup shown in Fig. 1(a). A strong, broad absorption feature centered at 1095 cm^{-1} with a weak absorption band near 800 cm^{-1} were assigned to the asymmetric stretching and bending modes of Si–O–Si, respectively. As is common with SiO_x films grown at reduced temperature, IR spectra also contain features attributed to hydroxyl groups. Absorption at 958 cm^{-1} was attributed to the Si–OH stretching vibration. Considering this, the broad band between 3000 and 3700 cm^{-1} could probably be assigned to an O–H stretching vibration of associated SiOH species and isolated Si-OH groups.[1,8,9] Table 1 shows the most important peaks of this spectrum.

The C=O peak at 1630 cm^{-1} indicates the presence of bonded oxygen in the polymer, likely originating from molecular oxygen when exposed to air.[10]

The presence of carbon in the films is probably due to the incomplete decomposition of the TEOS precursor and carbon contamination from open air.[11] The presence of Si-O-C bonds from incomplete decomposition of the precursor is shown in Fig. 2(b), where the FTIR region between 800 to 1400 cm^{-1} is deconvoluted.

1. Effect of Nozzle−Substrate Distance

The effect of nozzle−substrate distance on the deposition rate is shown in Fig. 3. Deposition rate increased when nozzle-substrate distance decreased. In addition, the deposited area diminished with increased nozzle−substrate distance. The deposition rate depends on the density of fragmented TEOS precursors reaching the surface of the substrate. In the helium APP jet, we observed that electron density and atomic oxygen density are highest when close to the nozzle, and then they decreased when the distance from the plasma jet nozzle

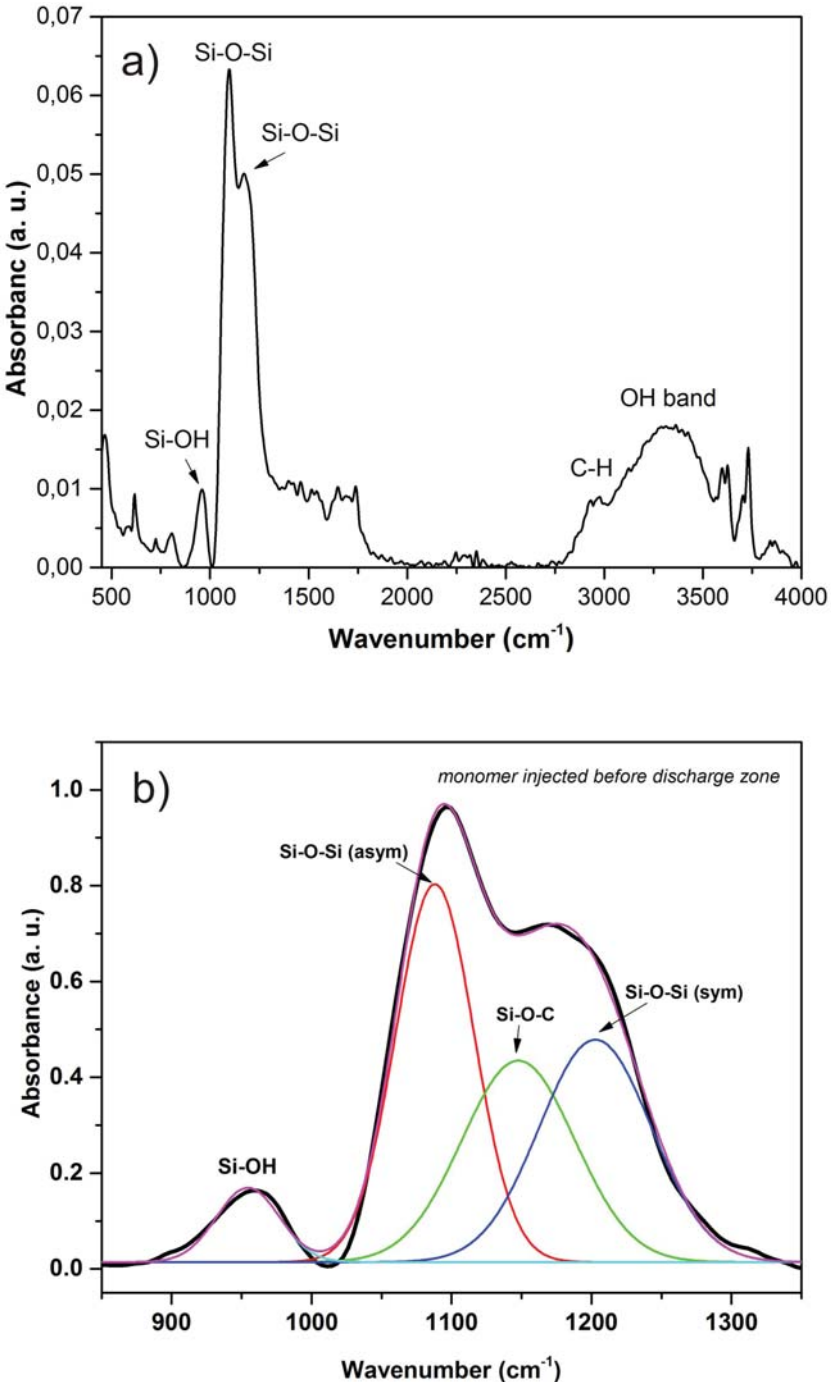

FIG. 2: (a) Typical absorption FTIR spectrum of silicon oxide–deposited film (monomer inlet before discharge zone); (b) typical Gaussian fitting curve of the spectrum in the range 800−1400 cm^{-1}

TABLE 1: Main peaks observed in ATR-FTIR spectra

Wave number (cm^{-1})	Vibrational mode
3000−3700	O–H Stretching vibration of associated SiOH
3000–2850	C–H Stretching, symmetric valence, and asymmetric valence modes
1171	Si-O-Si Symmetric stretching
1150	Si-O-C Asymmetric stretching
1095	Si-O-Si Asymmetric stretching
958	Si–OH Stretching

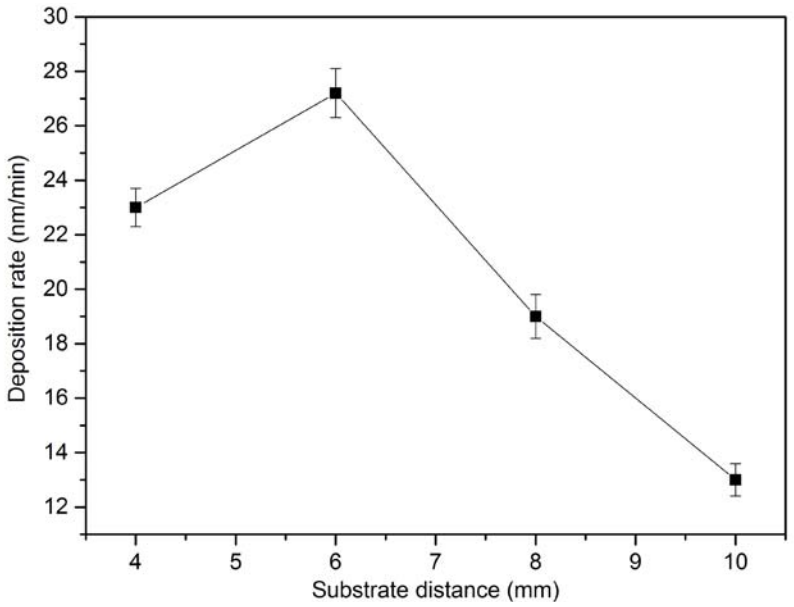

FIG. 3: Dependence of deposition rate on nozzle–substrate distance. Applied power, He gas flow rate, and deposition time: 2 W, 400 sccm, and 6 min, respectively

increased.[12] Thus, the density of the radicals formed from the fragmentation of TEOS may have also been reduced at greater nozzle−substrate distances, which explains the abrupt decrease of the deposition rate observed in Fig. 3 at > 6 mm. For distances < 6 mm, the deposited coatings show a certain inhomogeneity because of the distorted gas flow that occurred due to turbulence caused by the impact of the jet on the substrate surface. We can conclude that a short substrate distance is beneficial for a high deposition rate; however, for nozzle−substrate distances that are too short (< 6 mm), nonhomogeneous films (in terms of film thickness) were deposited. With our experimental conditions, nozzle−substrate distance of 6 mm was optimal because it resulted in a homogeneous and higher deposition rate.

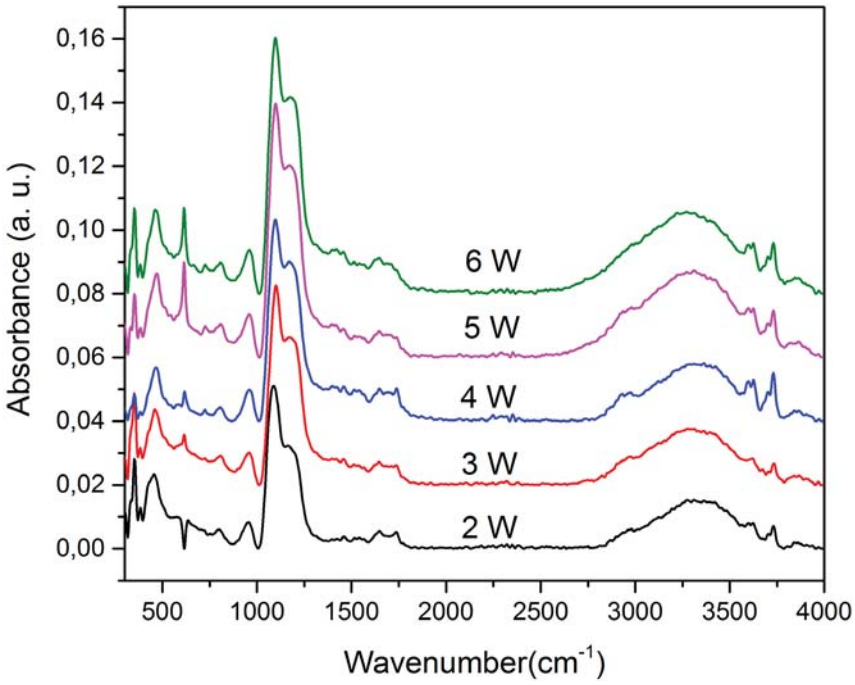

FIG. 4: ATR-FTIR spectra of films deposited at different applied powers

2. Effect of Applied Power

Figure 4 shows IR spectra of films deposited on a silicon wafer substrate, with applied power varying between 2 and 6 W. Si-O-Si peak intensity was higher for coatings deposited at higher applied power, leading to thicker coatings. Coatings deposited at lower applied power had a broad peak at 2700–3000 cm^{-1}, indicating the presence of a significant amount of carbon-related groups. Coatings deposited at higher plasma power were found to have higher silanol (SiOH) content observed at 958 cm^{-1}, which is associated with the formation of particulates. Increased deposition rate is most likely due to higher applied power that results in an increment in the fragmented radicals that occur after precursor fragmentation.

3. Effect of Deposition Time

Figure 5 demonstrates the thickness of the SiO_x films on the Si (100) substrates as a function of the deposition time. Film thickness tends to increase with deposition time in a linear manner.

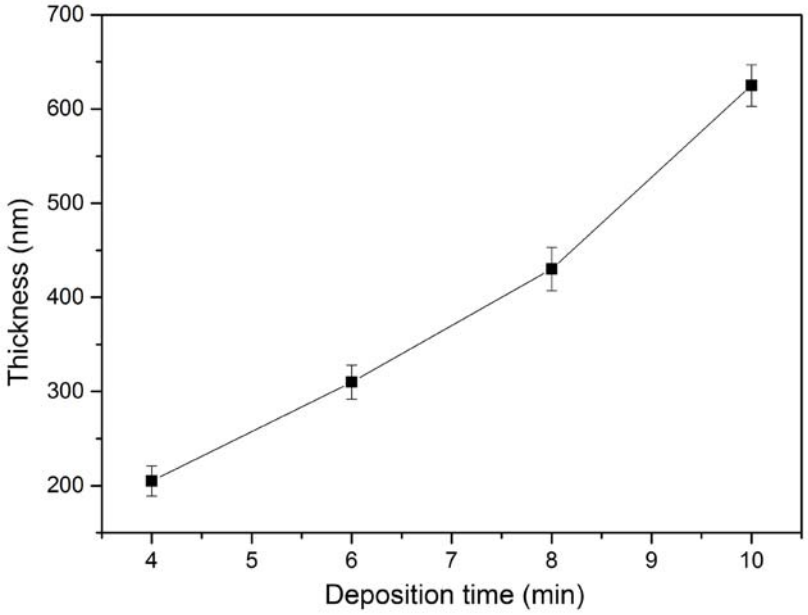

FIG. 5: Thickness of SiO_x film plotted as a function of deposition time. Applied power, He gas flow rate, and $d_{nozzle-substrate}$: 4 W, 400 sccm, and 6 mm, respectively

4. Effect of Precursor Inlet Position

The effect of precursor inlet position (Fig. 6) on deposition composition is shown in Fig. 6. When the precursor inlet position was close to the powered electrode, height of the shoulder corresponding to Si-O-Si increased. Figure 7 identifies the deconvolution of the spectral range between 800 and 1400 cm^{-1}, vibration peaks due to Si-O-Si bonds silanol (Si-OH) groups, and Si-O-C bonds. The coatings' carbon content is reduced when the monomer inlet is close to the tube outlet. This shows the role of atomic oxygen and OH radicals that can contribute to a higher fragmentation of the precursor.

We also examined surface morphology of SiO_x coatings in different applied powers using SEM (Fig. 8). It is evident that film thickness increased with increased applied power. SEM analysis of deposited thin layers obtained from the transporting discharge showed that the coatings' border region had a smooth morphology that became denser with increased applied power (Fig. 8[a]−[e]). The center of the coatings had individual particulates in the range of 200 nm−5μm in diameter, depending on power (Fig. 8[c], [f]). The formation of these particulate regions is a consequence of plasma jet tip collision on the sample. The increase in particulate size with higher applied power could be explained by augmented electric field at the plasma jet tip. As a result, coatings deposited at higher powers exhibited increased surface-roughness values at the center, but coatings at the borders were smooth and homogeneous (see Fig. 8[a]–[e]).

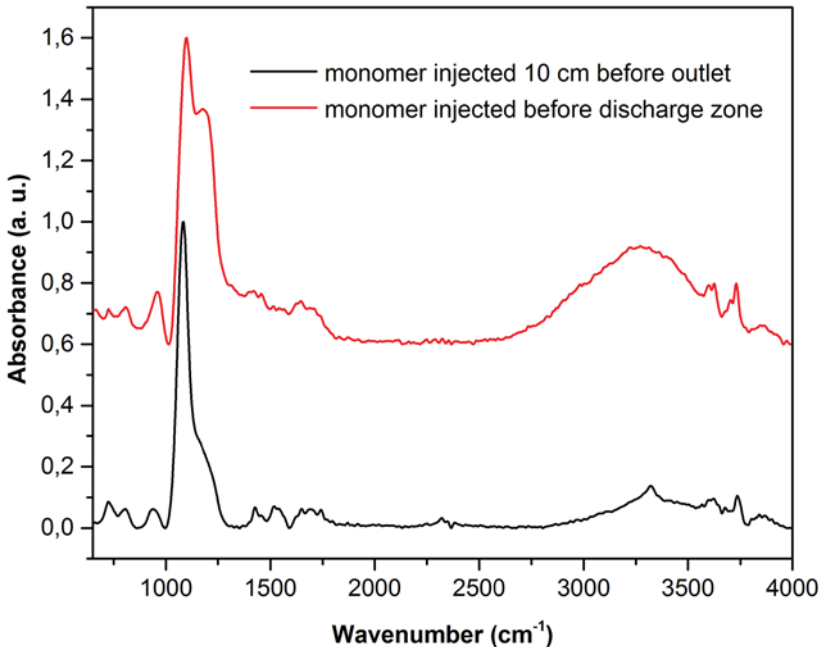

FIG. 6: FTIR spectra of SiO_x-deposited film for two different monomer injection setups

B. Deposition of Thin SiO_x Films inside the FEP Tube

We analyzed the chemical structures of the plasma-polymerized SiO_x films in the 70-cm FEP tube (D_{in} = 4 mm; D_{out} = 6 mm) using FTIR spectra in different parts of the tube (Fig. 9). FEP is a fluorinated copolymer obtained from copolymerizing hexafluoropropylene and tetrafluoroethylene. The TEOS precursor was injected before the discharge zone, because the purpose was to deposit inside the entire tube (Fig.1[a]). Samples were denoted according to distance downstream, with respect to the powered electrode at either 5 cm downstream (close to the HV electrode) or 65 cm downstream (close to the jet outlet).

Analysis of the deposited coatings inside the FEP tube using ATR-FTIR spectra indicated an SiO_x-type coating with the presence of characteristic absorption vibrations of Si-O-Si bonds inside the coatings. After 20 cm downstream (with respect to the powered electrode), spectra showed peaks corresponding to the FEP substrate at 1144 and 1200 cm^{-1} that were associated with the stretching vibration of the $–CF_2$ and $–CF_2$-CF_2 structures. This implies that the coatings close to the powered electrode are thicker than those deposited close to the jet outlet, because the corresponding peaks of FEP appear in the ATR-FTIR spectra. However, the thickness of SiO_x coatings seemed to be homogeneous up to a tube length of 35 cm.

To verify the surface morphology and film thickness inside the tube, we observed the SiO_x films using SEM. Figure 10 shows SEM images of the films deposited by

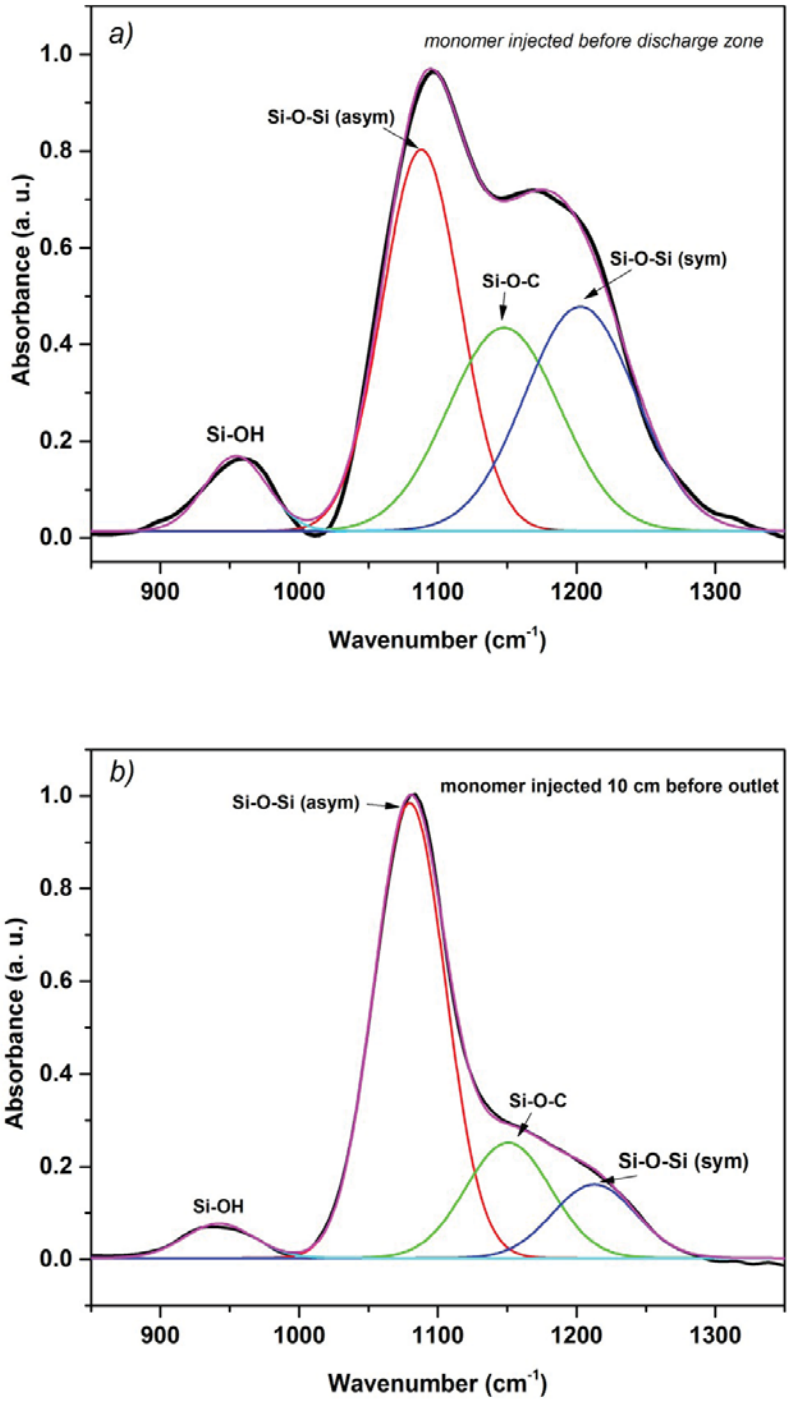

FIG. 7: Typical Gaussian fitting curve of spectra in the range 800−1400 cm^{-1}. (a) Monomer injected before the discharge zone; (b) monomer injected 10 cm before outlet

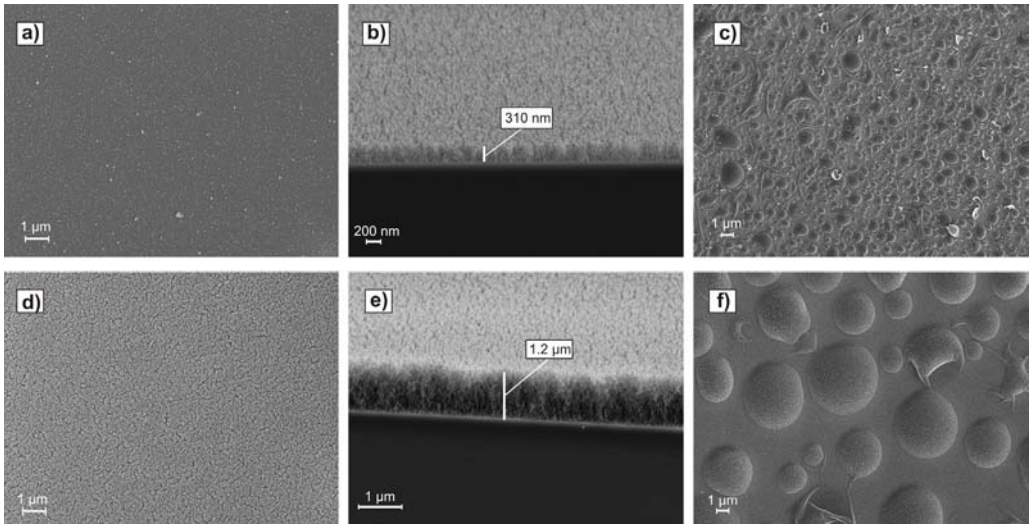

FIG. 8: Cross-sectional and top-view SEM images of deposited films for different applied powers. (a–c) P = 4 W; (d–f) P = 6 W. Plasma conditions: He gas flow = 400 sccm; t = 6 min; $d_{nozzle-substrate}$ = 6 mm.

the transporting discharge inside the tube. The film surface within the first 35 cm was smooth and continuous; no cracks were observed over that entire area. However, we observed some submicron silica particles on the films due to particulate generation near the outlet at 65 cm downstream. These may have originated from homogeneous nucleation, ion-induced nucleation, and air contamination near the outlet.[12]

The SiO_x-film deposition rate gradually decreased from the electrode to gas outlet, confirming the ATR-FTIR spectra observation. This can be attributed to the concentration gradient of the precursor radicals along the gas flow. The wettability of the SiO_x-coated FEP tube inner surface is presented in Fig. 11. FEP tube wettability increased after film deposition on the inner wall of the tube at all of the positions along the tube. This was shown by a water droplet completely wetted inside the FEP tube.

1. Cell Adhesion on SiO_x Coating inside the Tube

We examined cell adhesion of CT-26 cells on bare and coated FEP tubes. No adhesion of CT-26 cells was found to occur inside the tubes, but by changing the surface chemistry inside the tubes with deposition of SiO_x coatings (by PECVD from TEOS), cell-adhesive coating occurred (He flow rate, 400 sccm; TEOS flow rate, 0.2 sccm). The procedure was as follows: After deposition, the first 65 cm of tube were cut into three 20-cm long parts, which were used for cell culturing. Then, we injected 5 mL of CT-26 cell suspension with a density of 10^5/tube into the noncoated and coated tubes that were incubated at physiological conditions for 48 h. Finally, the biological

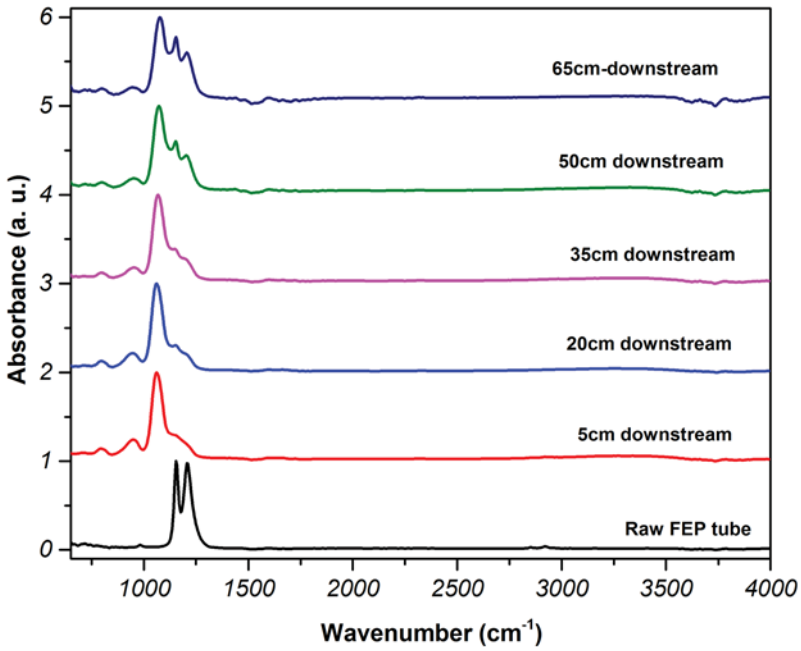

FIG. 9: FTIR Spectra of plasma-polymerized SiO_x coatings at different downstream positions inside the FEP tube. Plasma conditions: He gas flow = 400 sccm; deposition time = 90 min.

response to the plasma-deposited coating was investigated in vitro by trypsinating and counting CT-26 cell lines. As shown in Fig. 12, the bare (untreated) FEP tube showed no adhesion to CT-26 cells. On the contrary, most of the cells on SiO_x coating were attached in the tube. We counted the adherent cells and the resulting values of adherent cells were averaged.

As expected, we observed more cell adhesion on plasma SiO_x coatings, which were also stable after 48 h of cell culture. As the distance from the HV electrode increased, cell adhesion decreased. Measurements show that at a distance of 45−65 cm downstream from the tube, the coatings' nonadherent properties increased. A decrement of cell adhesion is probably due to the fact that the tube is not completely covered homogeneously because of the role of air regarding film growth and structure. Indeed, in such cases due to nonhomogeneity of coatings, cells will not only be in contact with coatings but also with the uncoated FEP substrate. Thus, the total number of counted cells decrease.

IV. CONCLUSIONS

APP treatment is a simple, inexpensive process that is useful for a wide variety of applications, including surface modification and deposition of coatings. In this ar-

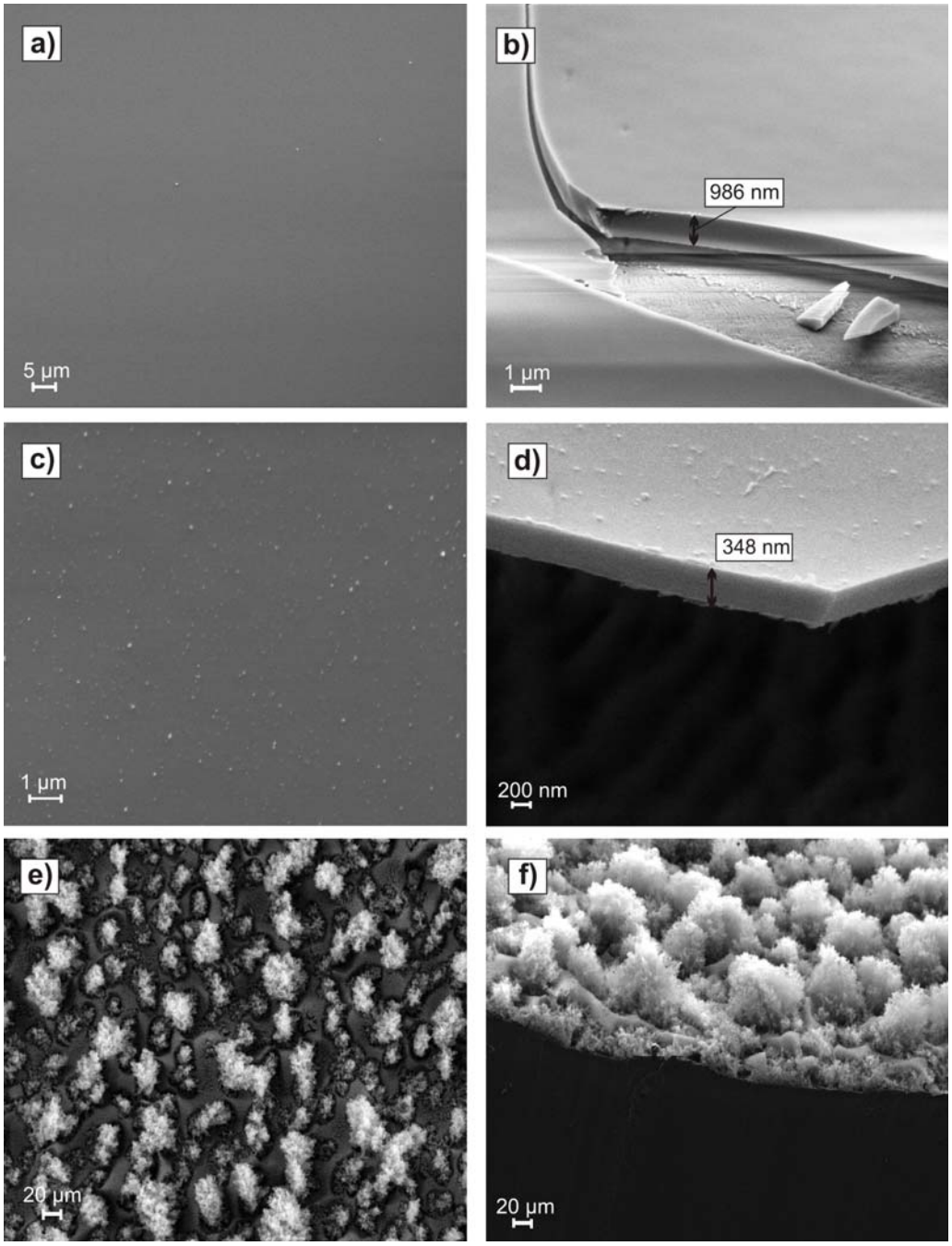

FIG. 10: Plane SEM and cross-sectional SEM images of SiO_x film deposited inside the FEP tube. (a, b) Five cm downstream (close to the HV electrode); (c, d) 35 cm downstream; (e, f) 65 cm downstream (close to the jet outlet)

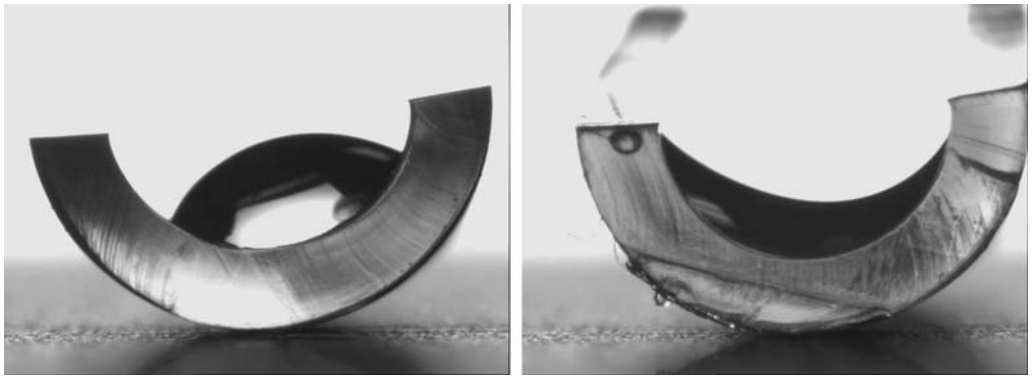

FIG. 11: Wettability on inner wall of plasma-treated FEP capillary (right) and untreated FEP surface (left). Droplet volume is 6 μL

ticle, we pointed out that long-distance traveling plasma has the ability to deposit thin films at atmospheric pressure. In addition, low temperature was used with a plasma jet to coat samples placed outside of flexible tubes and to coat inside commercial flexible tubes. SiO_x coatings were successfully deposited outside and inside of tubes. The chemical composition of films deposited on substrates that were

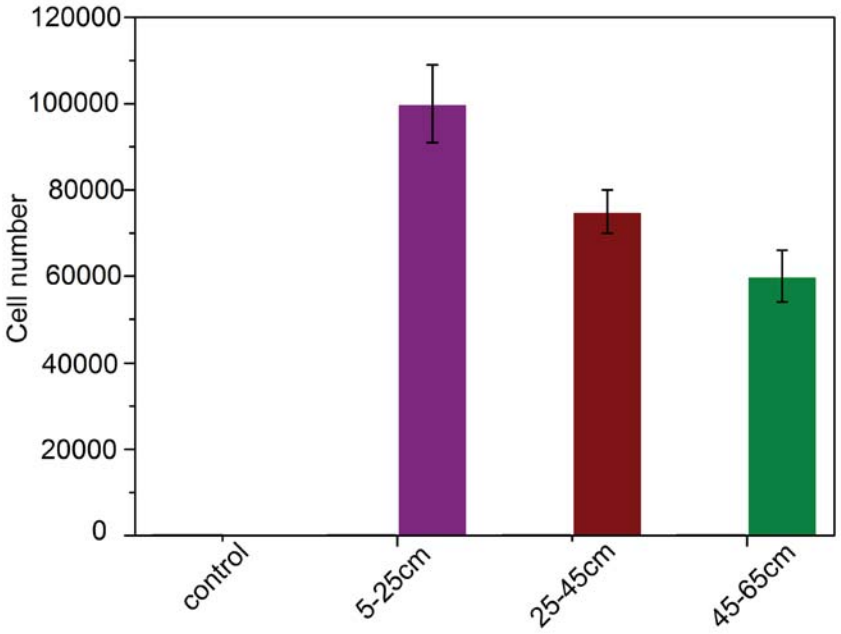

FIG. 12: Cell adhesion properties of CT-26 on SiOx coating incubated for 48 h in different parts of FEP tube

placed outside of the tube was found to depend on applied power, time, and monomer inlet position.

Coatings inside of tubes present a certain thickness gradient; however, SiO_x coatings completely modify the wettability inside FEP tubes. The wettability of Si substrates placed outside of tubes and covered by SiO_x coatings was also enhanced, in comparison to the untreated sample. The deposition rate of SiO_x films gradually decreased from the electrode to gas outlet. The film was smooth along the tube, but because of near-outlet particulate generation and influence of air, some silica particles were observed on the film.

Cell-nonadhesive or -adhesive properties of SiO_x coatings were evaluated by seeding CT-26 cell lines, which grow readily on films deposited at different parts inside of the tube. The cell-adhesion rate is reduced for longer distances and near the outlet, where the coating is very rough and does not cover the FEP tube completely. This may be due to monomer gradient and reduced film thickness at greater distances as well as the role of air close to the nozzle exit. From these results, we conclude that transporting discharge offers a great potential for modifying surface properties inside of catheter tubes that are used for evacuation of pathogen biological liquids.

REFERENCES

1. Babayan SE, Jeong JY, Schütze A, Tu VJ, Moravej M, Selwyn GS, Hicks RF. Deposition of silicon dioxide films with a non-equilibrium atmospheric-pressure plasma jet. Plasma Sources Sci Technol. 2001;10(4):573.
2. Favia P, d'Agostino R. Plasma treatments and plasma deposition of polymers for biomedical applications. Surf Coat Technol. 1998;98(1–3):1102–6.
3. Vasquez-Ortega M, Ortega M, Morales J, Olayo MG, Cruz GJ, Olayo R. Core–shell polypyrrole nanoparticles obtained by atmospheric pressure plasma polymerization. Poly Int. 2014;63(12):2023–9.
4. Ermakova E, Rumyantsev Y, Shugurov A, Panin A, Kosinova M. PECVD Synthesis, optical and mechanical properties of silicon carbon nitride films. Appl Surf Sci. 2015;339:102–8.
5. Prat R, Koh YJ, Babukutty Y, Kogoma M, Okazaki S, Kodama M. Polymer deposition using atmospheric pressure plasma glow (APG) discharge. Polymer. 2000;41(20):7355–60.
6. Sohbatzadeh F, Omran AV. The effect of voltage waveform and tube diameter on transporting cold plasma strings through a flexible dielectric tube. Phys Plasmas. 2014;21(11):113510.
7. Omran AV, Sohbatzadeh F, Siadati S, Colagar AH, Akishev Y, Arefi-Khonsari F. Single channel atmospheric pressure transporting plasma and plasma stream demultiplexing: Physical characterization and application to E. coli bacteria inactivation. J Phys D Appl Phys. 2017;50(31):315202.
8. Theil JA, Tsu DV, Watkins MW, Kim SS, Lucovsky G. Local bonding environments of Si–OH groups in SiO_2 deposited by remote plasma-enhanced chemical vapor deposition and incorporated by postdeposition exposure to water vapor. J Vac Sci Technol. 1990;8(3):1374–81.
9. Aumaille K, Vallée C, Granier A, Goullet A, Gaboriau F, Turban G. A comparative study of oxygen/organosilicon plasmas and thin $SiO_xC_yH_z$ films deposited in a helicon reactor. Thin Solid Films. 2000;359(2):188–96.
10. Gengenbach TR, Chatelier RC, Griesser HJ. Characterization of the ageing of plasma-deposited polymer films: Global analysis of X-ray photoelectron spectroscopy data. Surf Int Anal. 1996;24(4):271–81.

11. Zhu X, Arefi-Khonsari F, Petit-Etienne C, Tatoulian M. Open air deposition of SiO_2 films by an atmospheric pressure line-shaped plasma. Plasma Proc Poly. 2005;2(5):407–13.
12. Han MH, Noh JH, Lee TI, Choi JH, Park KW, Hwang HS, Baik HK. High-rate SiO_2 deposition by oxygen cold arc plasma jet at atmospheric pressure. Plasma Proc Poly. 2008;5(9):861–66.